A RATIONAL FIBRE PACKING DESCRIPTION TO MODEL AND PREDICT THE EFFECTIVE DIFFUSIVITY/CONDUCTIVITY OF A TRANSVERSELY RANDOM UD COMPOSITE: AN ANALYTICAL AND NUMERICAL-BASED APPROACH

S. Joannès[1], E. Hervé-Luanco[2,1]

[1]MINES ParisTech, PSL - Research University, MAT - Centre des Matériaux, CNRS UMR 7633,
BP 87, 91003 Evry Cedex, France
Email: sebastien.joannes@mines-paristech.fr
[2]Université de Versailles, Saint-Quentin en Yvelines,
45 Avenue des Etats-Unis, F-78035 Versailles Cedex, France
Email: eveline.herve@mines-paristech.fr

Keywords: Homogenization, Functionally graded materials, Fibre reinforced, Finite element, Generalized Self-Consistent Scheme, Image analysis, Diffusion

Abstract

This paper is based on a complementary approach between numerical and analytical modelling and investigates the transport phenomena acting in transversely isotropic multi-phased materials. The aim of this work is to take into account the effects of an interphase region and of the fibre arrangement on the effective diffusivity of unidirectional composite materials (UD). For this purpose an $(n + 1)$-phase Generalized Self Consistent Scheme (GSCS) has been developed and extended to a Morphological Representative Pattern (MRP) approach thanks to the use of "transfer matrices".
Microstructural Finite Element Modelling (FEM) helps supplying the analytical implementation. The effective diffusivity depends only on the diffusivity of each phase and on some microstructural parameters. In this paper, a single pattern application is dedicated to study the effect of the interphase region and two bi-phasic patterns are used to deal with fibre packing effect, where the needed morphological parameters are determined thanks to a simple cross-section image analysis. In that last case two kinds of matrix are considered: a diffusive one and another that is "trapped" by the fibres. Closed-form analytical expressions are provided.

Excerpt from ISBN 978-3-00-053387-7

1. Introduction

Regarding the transport phenomena modelling and focusing on the GSCS, a number of papers have already been published for uncoated or coated inclusions. Most evaluations and validations of these models involve comparisons with data in low or moderate volume fraction ranges. Since this family of models studies the behaviour of a single pattern embedded in a matrix, one can wonder about the model accuracy at higher concentrations where packing effects can no longer be neglected. In order to take into account the effect of fibre arrangement on the effective diffusivity, the multi-layered coated fibre problem presented in [1, 2] has been revisited in section 2 in order to be compatible with a MRP-based approach. Some "transfer matrices" have been introduced as in [3] to avoid tedious calculations. The effective diffusivity of a composite material made of multi-layered coated fibres embedded in a matrix is first derived thanks to the $(n+1)$-phase model and then to a MRP-based approach leading to closed-form estimates (section 2). Comparisons are made with FEM simulations in order to explore the scope of

applications of this analytical homogenization strategy. In section 3, the effect of an interphase region is thus studied for a hexagonal periodic arrangement of fibres and in section 4, a turnkey method is proposed to take into account a random fibre arrangement with induced confined matrix areas, in the specific case of insulated fibres. The only three parameters of the model can be determined from morphological image analysis of the UD composite cross-section.

2. Analytical and numerical-based modelling

2.1. Analytical foundations

The first step of the multiscale modelling of transport phenomena for materials with n-layered embedded fibres is to solve the problem of a n-layered cylindrical inclusion, embedded in an infinite matrix which is submitted to longitudinal or transversal homogeneous diffusion on its boundaries [4]. For this purpose the following "transfer matrices" have been used:

$$\mathbf{Q}^{(i)} = \prod_{\substack{k=i \\ i\geq k\geq 1}}^{1} \mathbf{N}^{(k)} \quad \text{and} \quad \mathbf{Q}^{*(n)} = \mathbf{J}^{(n)}(R_n)\mathbf{Q}^{(n-1)} \tag{1}$$

with

$$\mathbf{N}^{(i)} = \left[\mathbf{J}^{(i+1)^{-1}}(R_i)\,\mathbf{J}^{(i)}(R_i)\right] \tag{2}$$

and where $\mathbf{J}^{(i)}(r)$ is given by:

$$\mathbf{J}^{(i)}(r) = \begin{bmatrix} r & \dfrac{R_{i-1}^2}{r} \\ -D_T^{(i)} & D_T^{(i)}\dfrac{R_{i-1}^2}{r^2} \end{bmatrix} \tag{3}$$

In the studied n-layered cylindrical inclusion problem, phase (1) constitutes the central core and phase (i) lies within the shell limited by the two concentric cylinders with the radii R_{i-1} and R_i, $i \in \{1, 2, \ldots, n+1\}$, $R_0 = 0$ and $R_{n+1} \to \infty$. $D_L^{(i)}$ and $D_T^{(i)}$ denote respectively the longitudinal and transverse diffusivities of phase (i), and f_i the volume fraction of phase (i).
The different results of this problem have been combined with a self consistent equation leading to the prediction of the $(n+1)$-phase model (one pattern approach):

$$D_L^{\text{eff}} = \sum_{i=1}^{n} f_i D_L^{(i)} \text{ and, } D_T^{\text{eff}} = -\frac{\left[R_n Q_{21}^{*(n)}\right]}{Q_{11}^{*(n)}} \tag{4}$$

and also used to propose a MRP-based estimate (N_λ different patterns approach):

$$D_L^{\text{eff}} = \sum_{i=1}^{n} f_i D_L^{(i)} \text{ and, } D_T^{\text{eff}} = \frac{\displaystyle\sum_{i=1}^{n} f_i D_T^{(i)} \sum_{\lambda=1}^{N_\lambda} m_\lambda \frac{Q_{11}^{(i_\lambda-1)}}{Q_{11}^{(n_\lambda)}}}{\displaystyle\sum_{i=1}^{n} f_i \sum_{\lambda=1}^{N_\lambda} m_\lambda \frac{Q_{11}^{(i_\lambda-1)}}{Q_{11}^{(n_\lambda)}}} \tag{5}$$

where $Q_{11}^{(n_\lambda)} = \dfrac{Q_{11}^{*(n_\lambda)}}{2R_{n_\lambda}} - \dfrac{Q_{21}^{*(n_\lambda)}}{2D_T^{\text{eff}}}$. m_λ, i_λ and n_λ denote respectively the volume fraction of pattern λ, the number of the phase which corresponds to phase (i) within the λ pattern and the number of phases inside pattern λ. It is worth noting that D_T^{eff} is given in (Eq. 5) by an implicit function because $Q_{11}^{(n_\lambda)}$ depends on D_T^{eff}.

Excerpt from ISBN 978-3-00-053387-7

Let us consider now the two morphologically representative pattern-based approach ($N_\lambda = 2$ and $n_\lambda = 2$) presented in (Fig. 1) where in pattern 1, phase 1 lies inside phase 2 and in pattern 2, phase 2 lies now in phase 1.

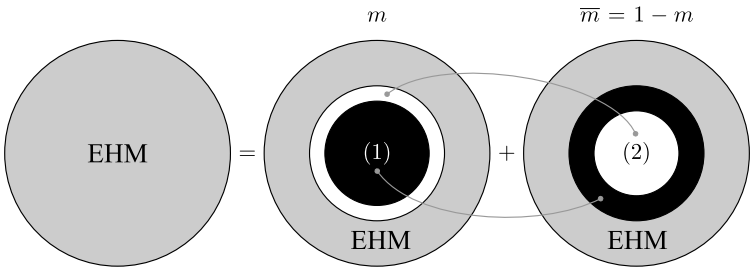

Figure 1. Two morphologically representative patterns.

For $D_T^{(1)} = 0$ and $D_T^{(1)} \to \infty$, $D_T^{\text{eff}}/D_T^{(2)}$ is no more given by an implicit function and becomes the following rational fractions:

$$\left.\begin{aligned} \frac{D_T^{\text{eff}}}{D_T^{(2)}} &= \frac{m\,(1-f)\,(f-mc) - f\,(1-m)^2\,(1-c)}{f\left[2m\,(f-mc) + (1-m)^2\,(1+c)\right] + m\,(1-f)\,(f-mc)} \quad \text{when } D_T^{(1)} = 0 \quad (a) \\ \frac{D_T^{\text{eff}}}{D_T^{(2)}} &= \frac{m\,(1+f)\,(f-mc) + f\,(1-m)^2\,(1+c)}{m\,(1-f)\,(f-mc) - f\,(1-m)^2\,(1+c)} \quad \text{when } D_T^{(1)} \to \infty \quad (b) \end{aligned}\right\} \tag{6}$$

where $m = m_1$ denotes the volume fraction of pattern 1 and $f = f_1$ the whole volume fraction of phase 1 such that $m_2 = 1 - m = \overline{m}$ and $f_2 = 1 - f$. Let c be the volume fraction of phase 1 in pattern 1.

2.2. Comparison with finite element simulations

The previous analytical estimates have been compared to the (reference) results of a full field numerical homogenization method (FEM). Three types of fibre arrangements have been considered: hexagonal arrangements, artificial random realizations and finally a real microstructure that have been digitized. Details of the FEM simulations are described in [5].

As an example, let us consider that the aligned fibres are an insulating phase (1) dispersed into a diffusive matrix phase (2). Results of analytical predictions and FEM simulations are compared in Table 1. From

Table 1. $D_T^{\text{eff}}/D_T^{(2)}$ (assuming $D_T^{(1)} = 0$) evaluated from the GSCS model, $\left(D_T^{\text{eff}}/D_T^{(2)} = (1-f_1)/(1+f_1)\right)$ with f_1 denoting the inclusion volume fraction, from an hexagonal periodic packing (FEM ⬡) and from artificial random realizations (FEM ■) with a uniform radii distribution for the fibres.

Fibre vol. fraction f	30%	40%	50%	60%	70%	80%
GSCS	0.538	0.429	0.333	0.250	0.176	0.111
FEM ⬡	0.538	0.428	0.333	0.248	0.172	0.100
FEM ■ (10 sim. average)	0.525	0.407	0.312	0.206	0.131	0.063
Corrected sample std. dev.	0.024	0.012	0.015	0.019	0.009	0.002

Excerpt from ISBN 978-3-00-053387-7

the first two result lines of Table 1 (GSCS and FEM ⬡) it can be deduced that, for a wide range of fibre volume fractions, a GSCS analytical approach seems to be particularly suited to predict the effective behaviour of a homothetic pattern-based microstructure[1]. Such a periodic and idealized fibre arrangement could be obtained on several metal matrix composites manufactured by a matrix coated fibre processing. As these well organized composites nevertheless involve more than two phases by presenting multilayered coated fibres and interphase areas, the n-layered approach is particularly appropriate to study the effect of an interphase region on the effective diffusivity, as it is depicted in section 3.

Comparing now the results of hexagonal packings (FEM ⬡) to those of artificial random realizations (FEM ■), reveals discrepancies from 30% (vol.) of fibres[2] that are mainly due to packing effects between inclusions as it is shown in Fig. 2. In that case, the introduction of only two appropriate morphological representative patterns as shown in (Fig. 1) is sufficient to take into account this particular fibre arrangement (see section 4).

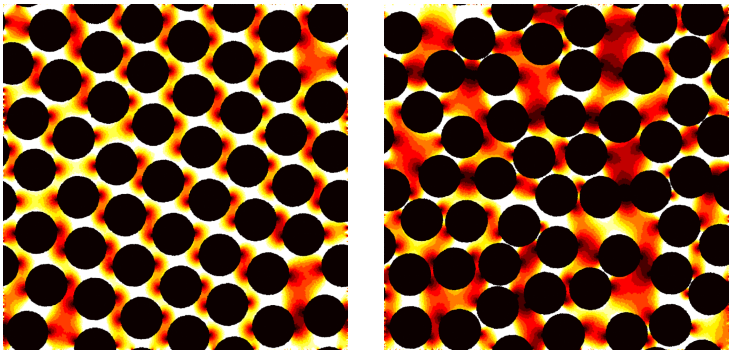

Figure 2. Norm of the flux, normalized between 0 (black) and 1 (white), resulting from an imposed periodic concentration gradient (horizontal direction) for two artificial random realizations with a fibre volume fraction of 60%. The left view shows a low perturbed hexagonal packing and the right view reveals packing effects and quasi-stagnant flow regions.

3. Effects of an interphase region on the effective diffusivity

In Fig. 3 the influence of the interphase has been studied by varying the volume fraction of phase 2 ($f_2 \in \{0\%, 10\%, 20\%, 30\%, 40\%\}$) and the contrast between the transverse diffusivities of the interphase and the matrix $D_T^{(2)}/D_T^{(3)}$. The inclusion volume fraction f_1 has been fixed equal to 30% and the transverse diffusion coefficient of phase 1 can either vanish or be infinite.
It is worth noting that the $(n+1)$-phase model allows also to take into account the effect of the presence of a gradient of property inside the interphase region such as for instance a distribution of porosity. An example of such a porous material is studied in [4].

4. A turnkey method to take into account the fibre packing effect

4.1. A model with only three parameters

To account for the fibre packing effect in composite materials with insulating fibres Eq. 6 (a) has been used. In this closed-form relation, three parameters are needed:

[1] As the hexagonal packing of inclusions is a particular example.
[2] Considering a uniform fibre diameter distribution, the relative error becomes maximum when $f \to \pi/2\sqrt{3}$.

Excerpt from ISBN 978-3-00-053387-7

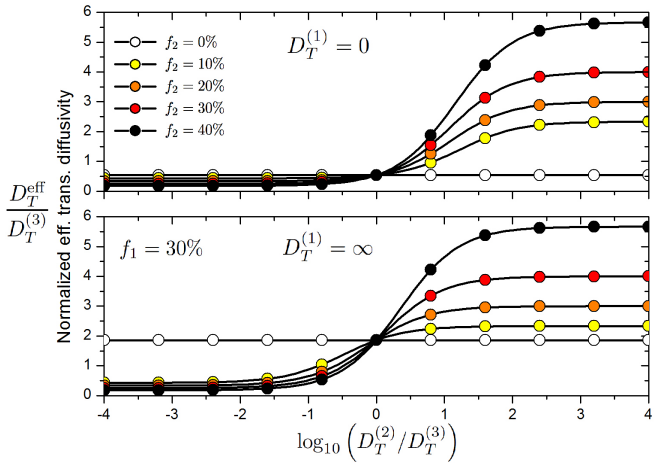

Figure 3. Effects of an interphase region (4-phase model with $f_1 = 30\%$) by varying the interphase concentration f_2 and the contrast between the diffusivities of the interphase $D_T^{(2)}$ and the matrix $D_T^{(3)}$. $D_T^{(1)}$ can either vanish (top) or be infinite (bottom)

- f, the fibre volume fraction.
- m, the volume fraction of pattern 1 which must be close to one for a hexagonal periodic arrangement[3] whatever the value of f. m can be seen as the volume fraction which does not lead to a screen effect and $\overline{m} = 1 - m$ might be regarded as an "ineffective diffusivity" volume fraction and corresponds to "dead volumes"; $\overline{m}$ is actually the volume fraction of zero flux areas. Depending on f, those areas might be associated to trapped matrix regions when $f > 0.5$ or to isolated rich matrix regions when $f < 0.5$.
- c, the volume fraction of fibres inside pattern 1, i.e. fibres associated to an "enveloping" matrix as opposed to fibres that "trap" the matrix.

When f and m are given, we have (see [5]):

$$0 \leq c_{\min} = 1 + \frac{f-1}{m} < c < c_{\max} = \frac{f}{m} \leq 1 \tag{7}$$

and consequently $m \geq 1/2 + |f - 1/2|$.

It is possible to plot Eq. 6 (a) in relevant ways. For given values of f and m, one can for example plot the normalized effective diffusion coefficient $D_T^{\text{eff}}/D_T^{(2)}$ (denoted $D_T^\star$ for convenience) versus c. As shown in Fig. 4, a network of curves (dashed lines) can be easily obtained by choosing several values of m and two envelope curves (solid lines) then appear. The relation between (m, c) pairs and the normalized effective diffusivity is not bijective, i.e. multiple (m, c) pairs might give the same value of $D_T^\star$.

The value of m is deduced from the following relation based on the study of the composite cross-section morphology:

$$m \widehat{=} m_{\min}^{(1-\widehat{m})} \tag{8}$$

[3] In this paper, m is considered equal to one in such a configuration.

Excerpt from ISBN 978-3-00-053387-7

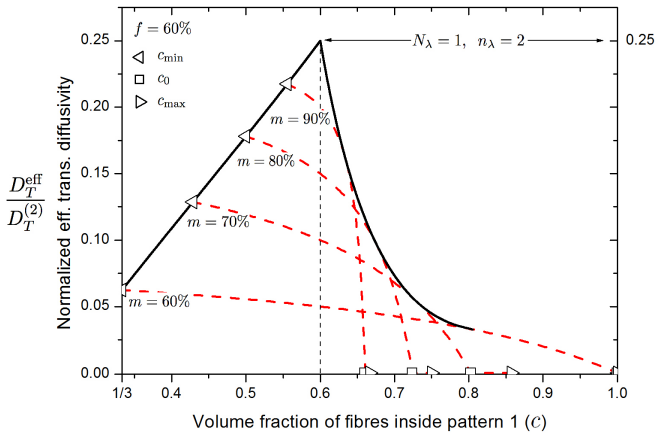

Figure 4. Biphasic case corresponding to Eq. 6 (a) with $f = 0.6$. The allowable set of pairs (m, c) are located between the two envelope curves (black solid lines).

where $\widehat{m}$ is obtained by an image analysis procedure (detailed in [5]) and is an indicator of the disorder degree depicted by m. An illustration of such an image process is given in Fig 5 where the grayed area corresponds to a measured ineffective diffusivity region.

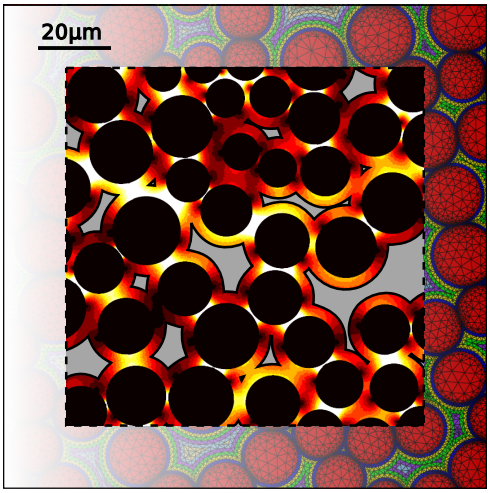

Figure 5. Norm of resulting flux, normalized between 0 (black) and 1 (white), resulting from a linear gradient concentration oriented along the horizontal direction. The grayed area corresponds to an ineffective diffusivity region and is obtained by a dilation operation of the fibres.

Since f and m are now given, it is possible to compute the allowed range for the c value. Two situations must be considered: for the lowest fibre volume fractions, c is necessarily small to ease the diffusion process whereas for the highest fibre volume fractions, c is large enough to reflect the difficulty of the matrix to percolate. It is thus necessary to balance the value of c between its bounds such that c tends to $c_{\min}$ when $f \ll 0.5$ and tends to c_0 when $f \gg 0.5$. The proposed weighting is based on the following

Excerpt from ISBN 978-3-00-053387-7

rule of mixtures:

$$c_{\text{weighted}} = (1 - f^a)\, c_{\min} + f^a c_0 \quad \text{with} \quad a = \frac{1}{(2f)^b}, \quad b \geq 0 \tag{9}$$

where $c_0 = \left[f\,(1-m)^2 - fm\,(1-f) \right] / \left[f\,(1-m)^2 - m^2\,(1-f) \right]$ and represents the upper limit of c when $D_T^{(1)} = 0$, i.e. $\lim_{c \to c_0} D_T^{\text{eff}} = 0$.

4.2. Validation of the model on a real microstructure

Let us study now the microstructure proposed in [6–8] and shown in Fig 5. This microstructure is made of glass fibres[4] embedded in an epoxy matrix. Following the image analysis procedure described in [5], the grayed region in Fig 5 corresponds to $1 - \widehat{m}$. An estimated value of m is thus obtained from $\widehat{m}$ using Eq. 8 and c_{weighted} is then computed according to Eq. 9 where $m = 0.96$ and b is taken[5] equal to 6.3. Applying closed-form relation Eq. 6 (a) allows to determine $D_T^\star \approx 0.17$ which is very close to the FEM results obtained on this microstructure. The relative difference between the reference and the analytical solution is only about 3%.

An empirical validation of the procedure could also be provided by this simulation. The grayed region indeed obtained by image analysis cover the matrix at a distance of more than 3 micrometers of the fibre edges. Empirical validation lies in the fact that the $D_T^\star$ result obtained previously is just slightly modified if the grayed area is now numerically considered as a non diffusive zone. In that case, $D_T^\star \approx 0.13$ and this value abruptly rises if only the layers above 4 micrometers are blocked (0.15), and even reaches a value of about 0.17 by considering that the ineffective layers are beyond 5 micrometers. Similarly the $D_T^\star$ value drops considerably (0.09) if all the layers above 2 micrometers are blocked. A kind of sharp transition zone seems thus to appear at a distance between 3 and 4 micrometers from the fibre edges. This shows that for a rich matrix region, only the matrix at the immediate vicinity of the fibres, which some called interphase, seems to be "active" for the transport properties.

Finally, one wonders what should be the effective diffusivity estimation carrying out a two steps procedure. This is equivalent to apply the single pattern GSCS approach followed by a classical self-consistent estimation. It remains the choice of the concentration for the first step which should be equal to c. By choosing c_{weighted} while keeping $m \approx 0.96$, one gets $D_T^\star \approx 0.21$ which is more than 22% of deviation. The application of the proposed one-step procedure with only 3% of deviation from the reference solution seems much more conclusive.

5. Conclusion

An n-layered Generalized Self Consistent Scheme (GSCS) coupled to a Morphologically Representative Pattern-based (MRP) approach has been used to evaluate the effective diffusivity tensor of random fibrous material composed of continuous unidirectional cylinders/fibres. Closed-form relations are given in the specific case of insulating fibres embedded within a diffusive matrix and, in that case, only two independent morphological parameters are needed to predict the transverse effective diffusivity of the composite. The fibre volume fraction f and the "effective diffusivity" volume fraction m are obtained through simple image analysis operations. A third (dependent) morphological parameter have been identified using FEM simulations and an excellent validation result has been obtained with a real microstructure.

[4] The fibre volume fraction is given by the author as 50% (vol.) but a higher local value, i.e. 60%, have been found by image analysis.

[5] Best fit with our numerical calculations (FEM ■) used to the parameter identification step.

Excerpt from ISBN 978-3-00-053387-7

References

[1] J. K. Lee and J. G. Kim. Generalized self-consistent model for predicting thermal conductivity of composites with aligned short fibers. *Materials Transactions*, 51(11):2039–2044, 2010.

[2] R. B. Yang, Y. M. Lee, Y. C. Shiah, and Tsung-Wen Tsai. On the generalized self-consistent model for the effective thermal conductivity of composites reinforced by multi-layered orthotropic fibers. *International Communications in Heat and Mass Transfer*, 49:55–59, 2013.

[3] E. Hervé and A. Zaoui. n-Layered inclusion-based micromechanical modelling. *International Journal of Engineering Science*, 31(1):1–10, 1993.

[4] E. Hervé-Luanco and S. Joannès. Multiscale modelling of transport phenomena for materials with *n*-layered embedded fibres. Part I: an analytical and numerical-based approach. *International Journal of Solids and Structures*, 2016.

[5] S. Joannès and E. Hervé-Luanco. Multiscale modelling of transport phenomena for materials with *n*-layered embedded fibres. Part II: investigation of fibre packing effects. *International Journal of Solids and Structures*, 2016.

[6] Y. Joliff, L. Belec, M. B. Heman, and J. F. Chailan. Experimental, analytical and numerical study of water diffusion in unidirectional composite materials - Interphase impact. *Computational Materials Science*, 64:141–145, 2012. Proceedings of the 21st International Workshop on Computational Mechanics of Materials (IWCMM 21).

[7] Y. Joliff, L. Belec, and J. F. Chailan. Modified water diffusion kinetics in an unidirectional glass/fibre composite due to the interphase area: Experimental, analytical and numerical approach. *Composite Structures*, 97:296–303, 2013.

[8] Y. Joliff, W. Rekik, L. Belec, and J. F. Chailan. Study of the moisture/stress effects on glass fibre/epoxy composite and the impact of the interphase area. *Composite Structures*, 108:876–885, 2014.

Excerpt from ISBN 978-3-00-053387-7